ISSN (Print) 1226-1750
ISSN (Online) 2233-6656
Journal of Magnetics 25(4), 441-452 (2020) https://doi.org/10.4283/JMAG.2020.25.4.441

Magnetic Relaxation Mechanisms in Ho Single Atom Magnets

Fabio Donati*

Center for Quantum Nanoscience, Institute for Basic Science (IBS), Seoul 03760, Republic of Korea
Department of Physics, Ewha Womans University, Seoul 03760, Republic of Korea

(Received 5 December 2020, Received in final form 8 December 2020, Accepted 8 December 2020)

Surface-supported single atoms with long magnetic lifetime, also called single atom magnets, represent the ultimate limit of downscaling of a magnetic bit. Due to the possibility to write, store and read information in their magnetic states, these atoms are model systems for future ultra-high-density magnetic storage devices. In this review, the properties of the most investigated single atom magnet, namely a Ho atom adsorbed on an ultrathin MgO film, will be presented together with the techniques used to address its quantum level structure and magnetic stability. The temperature and field dependent relaxation mechanisms of this unconventional magnetic system will be discussed based on recent findings. Finally, an overview of the open issues and possible future directions of the research will be provided.

Keywords : Single atom magnets, X-ray magnetic circular dichroism, Scanning tunneling microscopy, quantum magnets, surface spins, magnetic relaxation

1. Introduction

The constant need of increasing the storage density in magnetic memory media has been pushing the research towards the downscaling of a single bit, with the ultimate limit being a single magnetic atom. The requirements for a single atom to operate as a stable bit are summarized in the well-known magnetic recording trilemma, namely long thermal stability, efficient writability and large signal to noise ratio. For more than a decade, the research focused on finding the first example of single atom supported on a surface that can retain its magnetization for a time that is long enough to produce a hysteretic behavior with magnetic remanence [1-9]. This research led to the discovery of a new class of lanthanide-based one-atom materials, so-called single atom magnets [10, 11], which can retain their magnetization over thousands of seconds at cryogenic temperatures.

The present best and mostly investigated single atom magnets are Ho atoms supported on ultrathin films of MgO grown on Ag(100) single crystals, for which magnetic remanence is retained up to 40 K [10] and coercivity up to at least 9 T [12, 13, 14]. In addition to their remarkable magnetic stability, the magnetic states of these atoms can be addressed and controlled in magnetic transport measurements using scanning tunneling microscopy [12, 13, 15]. The possibility of storing, reading, and writing information in these atoms offers a unique platform for exploring single bit operation at the atomic scale.

After reaching the ultimate limit of magnetic storage, the research has been focusing on exploring the limit of magnetic stability of these materials and identifying the mechanisms that prevent a stable magnetization up to room temperature. By investigating the dynamics of magnetic fluctuations in these systems, it has been possible to unravel the effect of spin-phonon coupling [14], quantum tunneling of the magnetization [15], and the effect of the measurement process on the stability of the magnetic states of the atoms [10, 12]. The knowledge of these sources of magnetic relaxations will enable the design of more robust single atom magnets.

In this review, I will summarize the recent progress in this field, with particular focus on the magnetic relaxation mechanisms that affect the spin dynamics of Ho single atoms magnets. The paper will be organized as follows. The principles for stabilizing the magnetic moment orientation in single atom magnets will be presented in Chapter 2. In Chapter 3, I will summarize the structural,

*Corresponding author: Tel: +82-2-3277-2947
Fax: +82-2-3277-2947, e-mail: donati.fabio@qns.science

Invited Paper

electronic and magnetic properties of single Ho atoms on MgO/Ag(100). Chapter 4 will be devoted to the discussion of the characteristic magnetic relaxation mechanisms of these atoms, with emphasis on the spin-phonon interaction, quantum tunneling of the magnetization, and induced relaxation from the measurement procedures. Summary of the review and future perspectives will be given in Chapter 5.

2. Principles of Single Atom Magnets

The main difference between a single atom magnet and conventional lanthanide-based magnetic materials [16-20] is the absence of exchange interactions that couple the magnetic atoms to each other. Similarly to single ion molecule magnets [21, 22], in a single atom magnet the only interaction that can stabilize the orientation of the magnetic moments is the magneto-crystalline anisotropy generated by the chemical bonds with the surface atoms. In lanthanide atoms, this effect is mostly of electrostatic nature due to the strong localization of the 4f electrons around the nucleus and can be often modeled using a crystal field approach [23]. The broken translational symmetry offered by the surface is known to favor strong uniaxial anisotropy [1, 3, 5, 7, 8, 24]. In addition, the uniaxial component of the anisotropy can be particularly strong for atoms adsorbed on top of the oxygen site of MgO due to the axial chemical bond with the oxygen 2p orbitals [25-27].

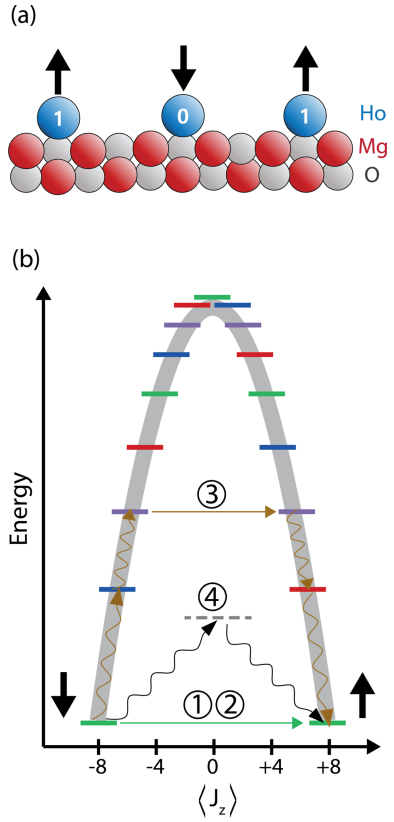

Fig. 1. (Color online) (a) Schematics of single Ho atoms adsorbed on the oxygen site of an MgO ultra-thin film. The orientation of their magnetization can be used as logic values (0 and 1). (b) Sketch of the magnetic levels of Ho atoms in the strong uniaxial crystal field of the oxygen adsorption site at the MgO surface. The transverse terms of the crystal field mix the state composition. The color code represents states that are linear combinations of the same subset of the m_j basis. Indicated in the figure are the 1) QTM, 2) direct process, 3) assisted QTM/Orbach process, and 4) two phonon Raman process.

For the case of Ho atoms at the oxygen binding site of MgO (Fig. 1a), the effect of the crystal field on the magnetic levels is sketched in Fig. 1b. When adsorbed on MgO, Ho atoms have a bulk-like $4f^{10}$ occupation [10]. Due to intra-atomic interactions, namely electron-electron exchange/correlation and spin-orbit coupling, states with maximum spin ($\boldsymbol{S}$ = 2) and orbital ($\boldsymbol{L}$ = 6) angular moments in parallel alignment are lowest in energy. Hence, the lowest multiplet of states is characterized by a maximum total angular momentum quantum number ($\boldsymbol{J}$ = 8). As shown in Fig. 1b, the degeneracy of the $2J+1$ states is lifted under the effect of the crystal field. The uniaxial component separates the 17 states into 8 doublets and 1 singlet according to their out-of-plane projection of the total angular momentum $\langle J_z \rangle = m_j$. The level splitting produced by the lowest order uniaxial term has a characteristic parabolic shape, with the ground state doublet having the largest m_j, see Fig. 1b. In this configuration, the atom magnetization is bi-stable and the two spin orientations define the 0 and 1 states of the atomic bit, as sketched in Fig. 1a. Higher order anisotropy terms may distort the parabolic level splitting and possibly stabilize a ground state doublet with intermediate m_j values [28, 29].

The quantization of the magnetic levels requires the exchange of energy and angular momentum with the surface to operate by discrete amounts, hence reversal of the spin orientation is only possible by "climbing the level ladder" in successive absorption of quanta from the substrate quasi-particles. For this system, the reservoir of quanta is mostly represented by MgO phonon modes [10]. Hence, the total level splitting provides an energy barrier that needs to be overcome to reverse the spin orientation. This energy barrier protects the atomic bit against undesired reversal events from thermal fluctuations, and its maximization is one of the primary requirements of a single atom magnet.

In addition to the strong uniaxial anisotropy generated by the bond with the underneath oxygen, the Ho magnetic

levels are perturbed by the presence of neighboring Mg and O atoms that generate transverse crystal field terms. The effect of these terms is to mix the composition of the magnetic states, whose representation becomes a linear combination of m_j states [23]. Depending on the symmetry of the crystal field, the representation of each level requires only a subset of the m_j states. Therefore, the multiplet of levels can be sorted in groups of states that are linear combination of the same m_j subset [30-32]. This level sorting is emphasized in Fig. 1b by assigning the same color to levels belonging to the same representation.

The main consequence of this level mixing is the opening of so-called underbarrier transitions, namely, transitions that allow reversing the direction of the spin without the need of reaching the top of the energy barrier. These processes can be classified in four categories:

1) Quantum tunneling of the magnetization (QTM): this process, first observed in polynuclear molecular magnets [33-35], triggers fluctuations of the ground state spin orientation when the magnetic levels are close to degeneracy. In case of large uniaxial anisotropy, it is mostly effective at zero field [34], although level degeneracy at finite magnetic field can also open additional quantum tunneling channels [11, 32]. This mechanism is essentially temperature independent and represents the main relaxation path at low temperature and zero magnetic field.
2) Direct processes: When the degeneracy between magnetic states is lifted, i.e., due to external magnetic field, the mixing provided by the transverse crystal field terms still allows direct transitions between the two ground state doublets. Differently from QTM, this mechanism requires the absorption or emission of an energy quantum. Hence, these transitions show a peculiar field and temperature dependent behavior [36].
3) Assisted QTM: upon absorption of one or more quanta of energy, the atom can reach an excited state for which QTM could be more effective than in the ground state. In this case, the energy required to reach the excited state represents an effective barrier for spin reversal, which is lower than the total barrier. After "crossing" the energy barrier, the system can relax to the lowest state with opposite m_j by emission of one or more quanta. Since this mechanism is limited by the absorption process, it typically shows an Arrhenius behavior with the temperature, with the effective barrier indicating the excited state to be reached to activate the QTM reversal [37, 38]. When only one quantum is involved in the absorption, this mechanism is often referred to as Orbach mechanism [36].
4) Two-phonon Raman processes: spin reversal can also occur upon simultaneous absorption and emission of two quanta, without the need of reaching an excited magnetic state. This process is conventionally represented by an absorption and emission via an intermediate virtual state (dashed line in Fig. 1b). In principle, these processes are available for an arbitrary energy quantum, hence a continuum of excitation is possibly generated, with the relative weight given by the phonon density of states, spin-phonon coupling and statistical population of the phonons [36]. These processes are generally characterized by a temperature power law whose characteristic exponent depends on the specific dimensionality and density of states. However, in case of strong contribution from non-dispersive local vibrational modes, the temperature behavior can largely deviate from textbook cases [39-41].

In order to minimize the impact of these underbarrier spin reversal mechanisms, it is crucial to minimize both the transverse crystal field terms responsible of level mixing, as well as the coupling between the spins and the phonon reservoir [38]. Practically, this is implemented by choosing a substrate that can offer strong uniaxial ligand configuration and low density of phonons. Remarkably, both features can be found in Ho atoms adsorbed on the MgO surface, as it will be discussed in the next section.

3. Ho Single Atom Magnets

3.1. Structural properties

In order to address the structural properties of Ho atoms

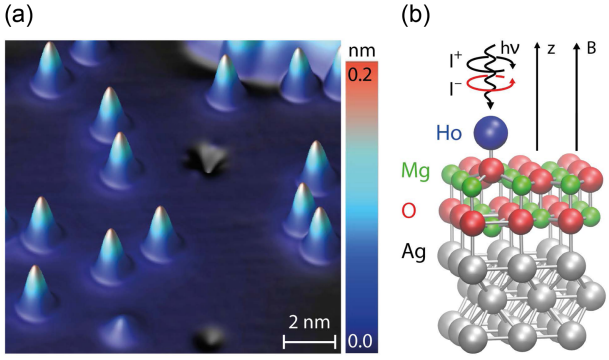

Fig. 2. (Color online) (a) Scanning tunneling microscopy image of Ho atoms on MgO/Ag(100). Tunnel voltage V_t = 100 mV, tunnel current I_t = 20 pA, T = 4.7 K, Ho coverage 0.005 ± 0.001 surface monolayer (ML). (b) Adsorption geometry of Ho atoms at the oxygen adsorption site of 2 ML MgO/Ag(100) obtained from DFT, together with a schematic of the XMCD measurement geometry. Adapted from [10].

on MgO/Ag(100), it is necessary to use an imaging technique with atomic resolution, such as scanning tunneling microscopy (STM) [42]. Figure 2a shows a 3D rendering of a typical STM image of the surface of 2 ML MgO/Ag(100) after deposition of Ho atoms [10]. The extreme reactivity of single atoms imposes the use of ultra-high vacuum conditions for both surface preparation and measurements. After preparation of ultrathin films of MgO on Ag(100) single crystals [10, 43, 44], single Ho atoms are sublimated using e-beam evaporator sources on the surface kept at around 4 K [10]. When deposited in these conditions, the large majority of Ho atoms adsorb on the oxygen site [44]. In addition, no diffusion occurs below a surface temperature of 50 K. This temperature represents the upper limit for structural stability of this system.

Figure 2b shows the calculated structure of these atoms from density functional theory (DFT) [10]. Upon adsorption on the surface, Ho forms a strong axial bond with the oxygen atom underneath that slightly deforms the lattice of the MgO. The short Ho-O bond length and the slight outwards relaxation of the oxygen atom is key to induce large uniaxial magnetic anisotropy with minimal transverse perturbation from the neighboring surface atoms.

3.2. Magnetic characterization with X-ray magnetic circular dichroism

The ensemble-averaged magnetic moments of Ho atoms projected along the surface normal can be measured with X-ray circular magnetic dichroism (XMCD) [10]. Synchrotron light sources are required for this experiment due to the need of measuring minute amount of lanthanide atoms (normally around 1-2 % of a single atomic layer) and of tuning the photon energy to resonant core level excitations [45, 46]. Using circularly polarized soft x-rays (schematics in Fig. 2b) at the M_{45} edges of holmium it is possible to excite core 3d electrons to the empty 4f states and probe their spin and orbital magnetic moments [7, 9, 10, 14]. By measuring the amplitude of the XMCD signal as a function of external magnetic field it is possible to record magnetization loops of the ensemble of Ho atoms [10]. As shown in Figure 3, an open hysteresis loop with remanence is observed at 6.5 K and up to 9 T. Open hysteresis is observed up to 40 K; at that temperature the loop is closed [10]. In the absence of ferromagnetic interaction between the atoms, this hysteretic behavior is the fingerprint of long magnetic lifetimes, as observed in single ion molecular magnets [37, 38, 47-52]. At low temperature, the characteristic spin fluctuations have a time scale that is longer than the measurement time of the magnetization loop (a full sweep

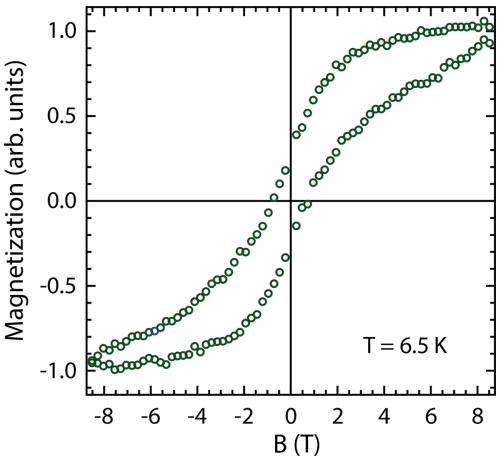

Fig. 3. (Color online) Magnetization loop M(H) of Ho atoms on MgO/Ag(100) obtained from the XMCD signal as a function of magnetic field. Field sweep rate dB/dt = 8 mT/s, photon flux $\Phi = 1\times10^{-2}$ nm^{-2} s^{-1}, T = 6.5 K, Ho coverage 0.01 ML, MgO coverage 7.0 ML. Adapted from [10].

can be done in the time scale of tens of minutes). Here, the dynamic of the magnetization of the ensemble is delayed with respect to the applied field, resulting in an out-of-equilibrium hysteretic behavior. The spin dynamic becomes faster with increasing temperature due to the increased amount of energy quanta from the phonon reservoir that accelerate the magnetic relaxation of the ensemble towards the thermodynamic equilibrium. At 40 K, the spin dynamic becomes fast enough to follow the external field, resulting in a fully paramagnetic loop [10].

A direct way to probe the long magnetic lifetime of these atoms is by directly recording the time evolution of the XMCD signal [35]. In order to record the decay of the magnetization at nearly zero field, a strong magnetic field is initially applied to saturate the ensemble along one orientation. Afterwards, the field is rapidly swept to 10 mT and the XMCD signal is recorded as a function of time. The magnetization of the ensemble shown in Fig. 4 exhibit a characteristic exponential decay whose time constant gives the magnetic lifetime of the Ho atoms. A value of about thousand seconds is recorded at 10 K [10]. The long lifetime at almost zero field suggests very small contribution to the magnetic relaxation from QTM, which is generally observed in systems with exceptionally strong uniaxial anisotropy [38] or predicted for atoms with specific ground states that are symmetry-protected against QTM spin reversal [30, 31]. Due to the exceptionally high coercivity of this system, the measurement of magnetic lifetime for Ho atoms on MgO/Ag(100) can also be performed at very high magnetic field. After saturating the magnetization along the negative orientation of the

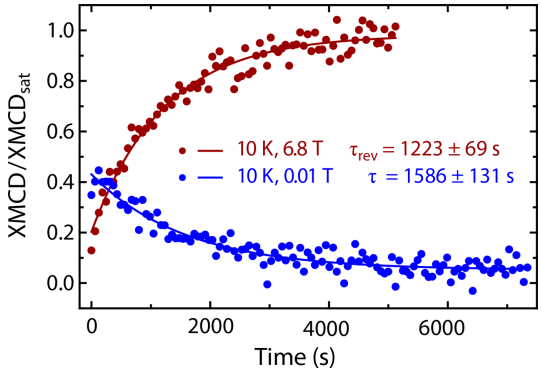

Fig. 4. (Color online) Time evolution of the maximum XMCD intensity (dots) normalized to the saturation value at B = +6.8 T. XMCD decay at B = +0.01 T (blue dots) was recorded after saturating the ensemble at B_{sat} = +6.8 T, while XMCD reversal at B = +6.8 T (red dots) was obtained after saturation at B_{sat} = -6.8 T. Ho coverage 0.015 ML, MgO coverage 6.0 ML, Φ = 0.14 × 10^{-2} nm^{-2} s^{-1}. Exponential fits (solid lines) give the magnetic lifetime τ and reversal time τ_{rev} of the Ho atoms. Adapted from [10]

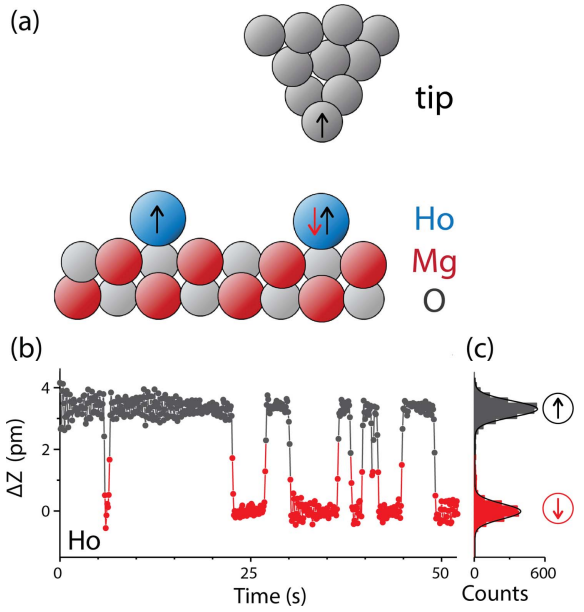

Fig. 5. (Color online) (a) Schematics of the tunneling magnetoresistance scheme in a spin-polarized STM experiment. Parallel/antiparallel alignment between the tip and the atom magnetization provide different values of the conductance and induce a change in the apparent height of the atom as measured in STM. (b) Two-level telegraphic signal recorded with a magnetic tip placed on top of the Ho atom. The tip was prepared by attaching Co atoms previously deposited on the surface. The telegraph signal in apparent height is due to magnetic switching of a Ho atom. (c) The histogram indicates a preference for one magnetization direction, identifying the magnetic ground state being up in the external field pointing up. B = 4 T, T = 4.3 K, V = 150 mV, I = 50 pA. Adapted from [13].

external field, the field is swept to maximum positive value and the evolution of the XMCD is recorded. Also in this case, an exponential behavior is observed, whose characteristic reversal time provides an estimate of the magnetic lifetime at high field. Even in large magnetic fields, the lifetime remains of the order of thousands of second at 10 K [10]. The field and temperature dependence of the magnetic lifetime of Ho atoms reveals characteristic magnetic relaxation mechanisms [14] that will be discussed in detail in Section 4.1.

3.3. Magnetic characterization using Scanning Tunneling Microscopy

Besides the remarkably long magnetic lifetime, Ho single atom magnets offer the possibility of individually accessing their magnetic state using STM [12]. Differently from conventional STM measurements, magnetic characterization requires the use of a magnetic tip that is used as a source of spin polarized electrons [53, 54]. The state of the atom can be read using a tunneling magneto-resistance scheme: the conductance of the junction depends on the mutual orientation of the tip and atoms magnetization. When a constant-current mode is employed, the fluctuation in the conductance results in a change of apparent height Δz, with the largest/lowest value of the apparent height corresponding to the parallel/antiparallel alignment of the magnetization [12, 13]. As shown in Fig. 5, typical telegraph signal is recorded when a magnetic tip is placed on top of a Ho atom. These fluctuations are attributed to the bi-stable behavior of the Ho atoms' electron spin fluctuating between the two lowest magnetic states (as represented in Fig. 1b). The timescale of these fluctuations provides insight in the dynamics of the spin under the effect of a transport measurement. It was observed that the Ho spin dynamics is affected both by the tunneling current and the bias applied between the tip and the sample, which defines the energy of the electrons flowing through the tunnel junction. The latter revealed three characteristic voltage thresholds that can be associated to energy thresholds (73 mV, 107 mV and 119 mV) required to reach excited states and trigger spin reversal. When a voltage below the lowest threshold is applied, no spin fluctuations are observed in the time scale of hours at 1 K [12] and only at 45 K spontaneous fluctuations in the time scale of 100 s are observed [13]. These results agrees with the values observed with XMCD and indicate a possible read and write scheme for the Ho atoms. Using low bias, it is possible to read the magnetic states without modifying it with the mea-

surement process. By applying a bias higher than the observed thresholds, it is possible to trigger spin reversal and set the magnetic state of the atom in the desired orientation [12, 13].

3.4. Magnetic level structure

By combing the full set of information obtained from XMCD and STM measurements, it is in principle possible to derive the level splitting of the magnetic states and further understand the origin of the remarkable magnetic stability of these atoms. However, the incomplete knowledge of the electronic configuration of the outer valence 6s5d shells does not allow one to fully determine the ground state of the system, and two different models could possibly explain the present set of findings [13]. The related level schemes are shown in Fig. 6. Both models assume a ground state with a total electron magnetic moment close to 10 μ_B as found in STM experiments [12]. If an unpaired electron was to populate the valence shell, the total magnetic moment would result from the sum of 4f and valence spins. To match the available data, this electron configuration would imply a magnetic ground state doublet with a 4f $\langle J_z \rangle = \pm 7$ (Fig. 6a). In the symmetry of the oxygen adsorption site, the atom would be protected by symmetry against quantum tunneling of the magnetization [10, 13, 41]. In case of absence of unpaired electrons in the valence shell, the magnetic moment would only be determined by the 4f electrons, resulting in a $\langle J_z \rangle = \pm 8$ ground state. For such a level structure, the low QTM rate could only be explained due to the large anisotropy barrier (around 180 meV) and large axiality of the system [55]. However, a finite QTM rate should be expected in the absence of external fields [15].

The knowledge of the static magnetic level structure is a fundamental information to determine the origin of the magnetic stability of Ho atoms, in particular against QTM. In addition to that, the spin dynamic at high temperature is strongly affected by the coupling between the phonon reservoir and the electron spins, as also observed in single molecule magnets [40]. Hence, particular effort has been devoted to identifying the impact of these two sources of magnetic relaxations on the spin dynamics of Ho atoms. The recent findings in these directions, together with the impact of the measurement techniques on the stability of the magnetic states, will be discussed in the next section.

4. Magnetic Relaxation Mechanisms

4.1. Phonon-assisted relaxation processes

Magnetic relaxation processes have been extensively studied in lanthanide based single ion molecule magnets [40] and paramagnetic compounds [36]. However, the peculiar absorption geometry of Ho atoms on MgO/Ag(100) with only one chemical bond connecting the magnetic atoms to the substrate represents an ideal platform to verify unconventional coupling mechanisms between the localized spins and the vibrational modes at the surface. Understanding of these mechanisms requires investigating the magnetic lifetime as a function of temperature and magnetic field. For this type of investigation, ensemble techniques such as XMCD are generally preferable as they allow collecting at once the average properties of a large number of atoms.

As discussed in Section 3, it is possible to directly

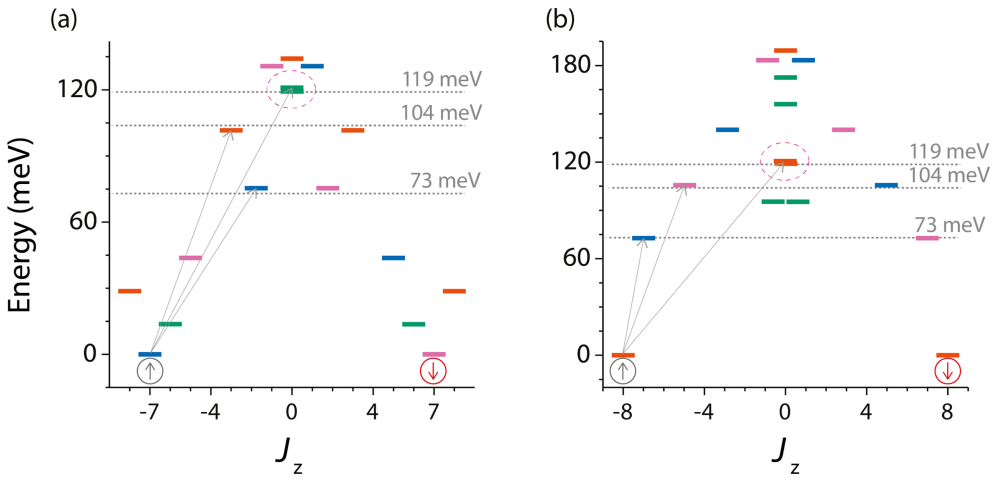

Fig. 6. (Color online) Energy level diagrams for the magnetic states of Ho atoms for the cases of (a) $J_z = \pm 7$ and (b) $J_z = \pm 8$ ground state for B = 10 mT. The arrows and the horizontal lines denote the three thresholds reported in [12]. Levels of equal color are connected via the fourfold symmetry. Circles indicate the most intense transitions producing spin reversal. Adapted from [13].

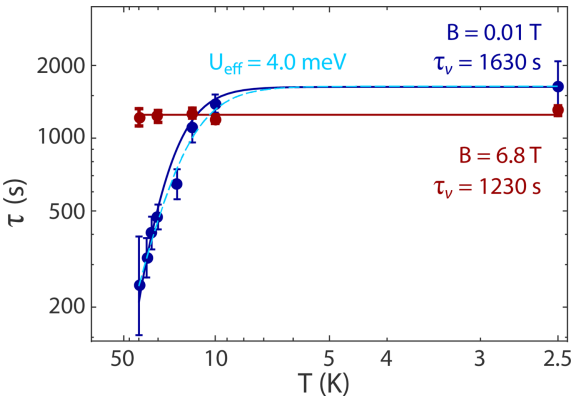

Fig. 7. (Color online) Magnetic lifetime τ versus temperature for B = 0.01 (blue dots) and B = 6.8 T (red dots). The cyan dashed line is a fit including an exponential process with effective barrier U_{eff} = 4.0 meV and a temperature-independent photon-induced relaxation with τ_v = 1630 s. Blue and red solid lines are fits to the low and high field data, respectively, using the two-phonon model involving local modes described in [14]. Adapted from [14].

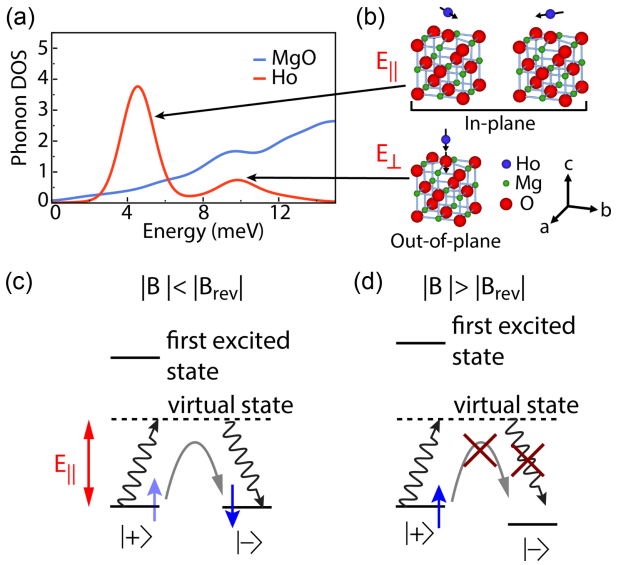

Fig. 8. (Color online) (a) Calculated phonon DOS projected onto the Ho atom and MgO slab. (b) Eigenvector of the modes involving large displacement of the Ho atoms. (c) Schematics of the two-phonon process for the thermally activated relaxation at low field and high temperature. (d) In high field, this mechanism is suppressed due to the energy splitting of the lowest states. Adapted from [14].

access the magnetic lifetime of the Ho atoms by recording the evolution of the XMCD as a function of time for a given value of the external magnetic field and temperature [14]. Figure 7 summarizes the results of this investigation. When measured at close to zero field, Ho atoms show two different regimes. At low temperature, the relaxation time is essentially temperature independent. It was found that, in this regime, the lifetime of the Ho atoms is limited by the measurement process itself rather than by intrinsic processes. As it will be discussed in Section 4.3, the absorption of soft X-rays in the substrates generates a large amount of hot photoelectrons than can scatter against the atoms and provide an effective relaxation pathway [10, 56, 57]. For temperatures above 10 K, the magnetic relaxation follows a characteristic exponential behavior. The exponent of this temperature-dependent function provides a value of the effective barrier of the process U_{eff} = 4.0 ± 1.0 meV. Relaxation mechanisms with exponential temperature dependence are often associated to so-called Orbach processes [36], where the absorption of a phonon leads to a magnetic excited state for which spin reversal is likely to occur (see also Section 2). However, for the case of Ho atoms, no excited magnetic state was found at this low energy value, with the first available state being at a few tens of meV (see Fig. 6) [13]. The magnetic lifetime behavior is even more unconventional for high values of the magnetic fields, where it appears to be essentially temperature independent over the whole accessible experimental range. This behavior is rather opposite to that of most of single molecule magnets, for which the magnetic lifetime decreases at higher field due to increasing relaxation rate from direct processes [40, 47-52]. In the case of Ho atoms, the main active mechanism at high field is the photon-induced relaxation, whereas the thermally-activated relaxation mechanism observed at close to zero field appears to be suppressed.

The peculiar behavior of Ho atoms can be rationalized by considering the vibrational properties of the coupled Ho/MgO system. According to DFT, the phonon density of states presents two localized modes at $E_{||}$ = 4.7 meV and $E_{\perp}$ = 8.6 meV that correspond to the in-plane and out-of-plane vibrations involving strong displacement of the Ho atom (see Figs. 8a and 8b). Remarkably, the energy of the in-plane modes matches well the experimental value of the effective barrier for spin reversal. This suggests that, within the timescale of the experiment, the main intrinsic relaxation mechanism can be attributed to the coupling between the Ho spin and this local mode.

In an early work [58], it was predicted that, in the presence of local vibrational modes with narrow energy lines, two-phonon relaxations involving these modes may produce a characteristic exponential behavior rather than a power law. Deviations from the expected power law characteristic of the two-phonon Raman process is often found in molecular magnets and generally ascribed to the

presence of local vibrational modes of the ligand involving the displacement of the magnetic ion [40, 41]. However, a pure exponential behavior was never reported. In the case of Ho single atom magnets, the simplified ligand environment allows a very clear identification of the vibrational modes that possibly couple to the Ho spins.

The rationale of this coupling is sketched in Fig. 8c and 8d. At close to zero field, the two ground state levels are degenerate. By absorption and emission of the same quantum of energy provided by the local mode, the Ho atom can flip its orientation. This process requiring the absorption of a specific quantum of energy, it gives rise to a typical thermal activation with exponential temperature dependence. At high field, the degeneracy between the two lowest levels is lifted, hence the same quantum of energy cannot connect the two states in the absorption and emission process. In this case, the reversal mechanism is suppressed. By analytically modelling the two-phonon process, it was possible to explain the available data with great accuracy, as shown in Fig. 7. Differently from what was found in paramagnetic bulk impurities [36], the model suggests that the continuum of dispersive MgO phonon modes have no significant contributions in the time scale of thousands of seconds, possibly due to the relatively small displacement that they induce on the Ho atoms [14]. This evidence reflects the differences in the surface versus bulk bonding environment for magnetic atoms.

The transition between the low-field and high-field regimes occurs at a specific field $B_{rev} \sim 0.2$ T which corresponds to the typical hyperfine field region, indicating that the coupling between nuclear and electron spins may also play a role in the magnetic relaxation process. This particular interaction, as it occurs at low fields, is often found to influence relaxation via QTM [59, 60]. This point will be discussed in the next section.

4.2. Quantum tunneling of the magnetization

The behavior of the Ho single atom magnets at low temperature and field was investigated using STM with the aim of precisely quantify the impact of QTM on the magnetic relaxation [15]. Instead of applying an external field with conventional magnets, the experiment took advantage of the stray field produced by the magnetic tip to locally sweep the magnetic field around the Ho atoms. The experiment was conducted as sketched in Fig. 8a. First, the magnetic state of the Ho atom was initialized in the desired configuration by applying a bias larger than the spin-reversal thresholds. The bias was then reduced, and the magnetic tip retracted for a certain amount of

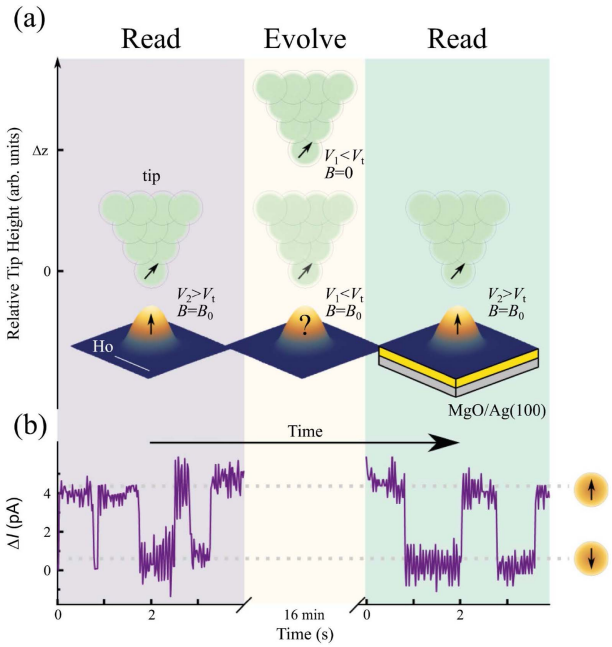

Fig. 9. (Color online) (a) Schematic of a magnetic STM tip (green) positioned above a Ho atom on MgO/Ag(100). It = 104 pA, V = −130 mV, white scale bar 2 nm. The magnetic state of Ho before and after its evolution is read by switching it with a tunnel voltage above the spin reversal threshold $|V_2| > |V_t| = 73$ mV (left and right panels). (b) Current traces showing two-state telegraph signal. $I_{set\text{-}point} = 100$ pA, $V_2 = -130$ mV, T = 4.7 K, feedback open. At tunnel distances, the antiferromagnetic tip exposes the atom to a stray field B_0; when sufficiently retracted, the field is essentially zero. In the example shown, the up state is preserved for 16 min at $|V_1| < |V_t|$ and $B = B_0$. Courtesy of Forrester *et al.* [15].

time (around ten minutes), to leave the magnetic state of the atom in the most unperturbed condition for evolution. The tip was then approached again, and the bias increased to perform a read-out of the magnetic state. The tip retraction and approach correspond to a field sweep from an initial value B_0 of about 100 mT to a negligible residual field, and back to the initial value B_0.

The correlation between the magnetic state before and after the field sweep reveals possible switching events to be attributed to QTM. The experiment reveals a finite number of switching events that increases when the number of tip field sweeps during the free-evolution period is increased from 1 to 20. As the tip field sweep cannot reverse the orientation of the magnetic field and cross the zero-field point, the increase of spin switching events with increased number of sweeps implies that QTM occurs at finite fields. Such an effect is normally possible for magnetic ions with non-zero nuclear spins, which is the case for Ho with 100 % natural abundance of

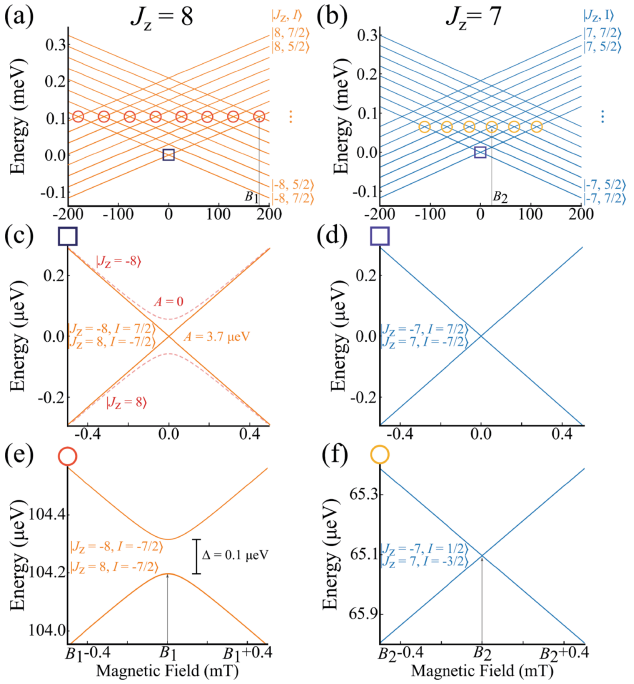

Fig. 10. (Color online) (a) Zeeman diagram for the $J_z = \pm 8$ ground state model. The red circles mark the level crossings at which QTM can occur. The dark-purple square indicates the lowest energy zero-field crossing. (b) Same as (a) for $J_z = \pm 7$ model. Here, gold circles mark the the level crossings with highest QTM rates found for molecular Ho systems, while the light-purple square mark the lowest energy zero-field crossing. (c) Lowest energy zero-field crossing with (solid orange) and without (dashed red) nuclear spin for the $J_z = \pm 8$ model. (d) Lowest energy zero-field crossings at zero field for the $J_z = \pm 7$ model. (e) Representative QTM level crossing for the $J_z = \pm 8$ model. (f) In contrast to the $J_z = \pm 8$ model, no first-order QTM level crossing are expected for the $J_z = \pm 7$ model. Courtesy of Forrester *et al.* [15]

nuclei with spin I = 7/2. As shown in Fig. 10, the hyperfine interaction between electron and nuclear spins generates a set of non-degenerate states whose energy evolves with the magnetic field according to their electron spin Zeeman energy. In the absence of hyperfine interaction, only one level crossing would be expected at exactly 0 T. Depending on the J_z value of the ground state, Ho atoms should (Fig. 10c) or not (Fig. 10d) exhibit QTM at 0 T, where the lowest states are degenerate. On the other hand, the hyperfine interaction in Ho couples the electron and nuclear spins in a 2(2I+1) multiplet of levels defined by their quantum numbers J_z and I_z. Over a region of about 200 mT, levels with opposite electron spin state cross at finite values of the applied field depending on the hyperfine coupling [28, 29]. Despite the large number of points producing level degeneracy, to first order only level crossing involving state with the same nuclear spin state allow for efficient QTM. These crossings are pointed in Fig. 10a and 10e. Remarkably, this situation is only possible for the model that assumes a $J_z = \pm 8$ states. In case of $J_z = \pm 7$ ground state (Fig. 10b and f), the electronic state is protected by symmetry, hence to first order no crossing point can lead to efficient QTM of the magnetization. The observation of QTM-related spin-switching suggests that the ground state of Ho atoms should have $J_z = \pm 8$, hence supporting the model shown in Fig. 6b.

4.3. Relaxation induced by the measurement process

The final mechanism to be discussed in this review concerns the impact of the measurement process on the stability of the quantum states, which is a relevant issue whenever the scale of the system reaches the atom size. Specifically, the probing mechanism in the two type of measurements, namely low energy tunneling electrons in STM measurements versus high energy photons in spatially-averaged ensemble XMCD, does affect the relaxation process. In STM measurement, the same Ho atom is continuously sampled by the flow of tunneling electrons. Although this probing mechanism may potentially trigger undesired spin-reversal events, the energy of these electrons can be controlled by the applied sample-tip bias. It has been shown that by accurately choosing the bias below well characterized thresholds, the atoms can be read without modifying the magnetic states [12]. At 1 K, Ho atoms do not show spontaneous switching on the timescale of days. This threshold behavior also enables a controlled writing protocol [12, 13, 15]. When the applied bias overcomes the identified thresholds, the rate of switching increases with the tunneling current. The process exhibits a power law with unitary exponent, which identifies the spin-reversal to occur via single electron excitations [12]. This evidence supports the interpretation of the reversal thresholds in terms of excited states enabling assisted QTM reversal [13].

In XMCD measurements, ensembles of the order of 10^{10} Ho atoms are probed in the spot size of the X-ray beam (around 1 mm^2) [10]. For the typical photon flux employed in the measurements, it was estimated that about 10^6 Ho atoms are probed every second [10]. Upon absorption of a high energy photon, the Ho atom reaches a short living excited state and is likely to decay in an uncorrelated magnetic state. Nevertheless, only a small fraction of atoms in the ensemble are sampled in the time scale of one spectrum or magnetization loop (minutes). Hence, the exposure to photons can be thought as a continuous sampling process that essentially measures the magnetization of "fresh" unsampled atoms, with minimal

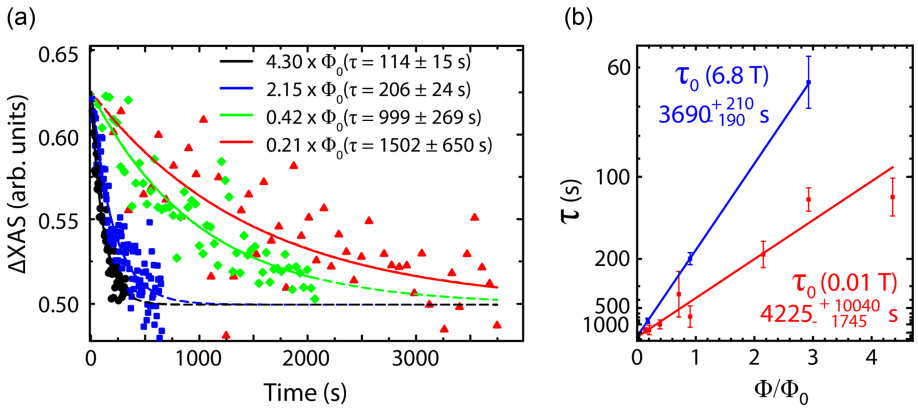

Fig. 11. (Color online) (a) Time evolution of the XAS intensity of a circular left polarization for different photon flux at B = 0.01 T and T = 2.5 K, after saturation at +6.8 T. Full curves are exponential fits to extract the magnetic lifetimes. All curves are rescaled to match the initial and the asymptotic value of the red curve. Ho coverage 0.01 ML, MgO coverage = 5.0 ML, $\Phi_0 = 1 \times 10^{-2}$ nm^{-2}s^{-1}. (b) Magnetization lifetime as a function of the photon flux at 0.01 T (red) and 6.8 T (blue). Linear regressions allow extrapolating the intrinsic lifetimes τ_0. Adapted from [10]

direct impact on the results of the measurement.

Even if the direct sampling of Ho atoms with photons does not represent a significant perturbation to the magnetization of the ensemble, the photon absorption in the substrate generates hot secondary electrons that can travel in the conduction band of the MgO and scatter against the Ho atoms, hence triggering spin reversal events. The number of secondary electrons is significantly larger than the photons directly absorbed by the Ho atoms, hence this process may have relevant impact on the lifetime of the magnetic states and influence the result of the XMCD measurement [10, 56, 57].

In order to estimate this effect, flux-dependent measurements of the magnetic lifetime were performed both at close to zero and high magnetic fields. As shown in Fig. 11a, the relaxation time at close to zero field increases when the photon flux is reduced. Similar effect is observed at high field. The flux-dependent measurements allow extrapolating the value of the lifetime at zero flux, which was found to be of the order of one hour both at low and high magnetic fields. Even at lowest photon flux that can be used to achieve a sufficient signal to noise ratio, the generated photoelectrons have in impact on the magnetic lifetime of Ho atoms and provide an upper limit of relaxation timescale that can be measured using XMCD.

5. Conclusions

In this review, I summarized the recent discoveries related to Ho single atom magnets on MgO/Ag(100) and the related magnetic relaxation mechanisms. These atoms represent at the moment a benchmark of magnetic stability for surface adsorbed spins. At the present state of the research, the key features for their magnetic stability seems to be the strong uniaxial ligand field provided by the oxygen adsorption site of the surface [10, 25, 26, 44], as well as the insulating character and low acoustic phonon density of the ultra-thin MgO film. Understanding the magnetic properties of the system and the relaxation processes at the MgO surface [14, 61] are crucial steps to engineer future atom bits and reach magnetic stability at ever higher temperatures.

To this extent, the knowledge of the 6s5d occupation is required to clarify the open point of the magnetic ground state of Ho atom and the related contribution of the valence electrons to the magnetism of the system. The presence of unpaired valence electrons is not only important to determine the stability of the magnetic states, but also to enhance the magnetic signal in tunnel transport measurements. In Dy single atom magnets on graphene/Ir(111) [11, 62, 63], the presence of an unpaired electron in the 6s shells enhances the magnetic contrast in STM measurements by more than an order of magnitude with respect to the signal from Ho atoms on MgO/Ag(100) [64]. In view of satisfying the requirements of the magnetic recording trilemma, an increased magnetic contribution to transport measurements could both enhance the signal to noise ratio in the detection as well the efficiency in writability of the atomic states.

Future works are expected to fully unravel the missing pieces of information for the Ho atoms, as well as to discover novel lanthanide single atom magnets on MgO and other supporting substrates with low electron and acoustic phonon densities, in the hope of identifying systems with enhanced thermal stability and optimized electronic configurations for single atom recording.

Acknowledgements

The author acknowledges funding from Institute of Basic Science, Korea through the Project No. IBS319 R027-D1.

References

[1] P. Gambardella, S. Rusponi, M. Veronese, S. S. Dhesi, C. Grazioli, A. Dallmeyer, I. Cabria, R. Zeller, P. H. Dederichs, K. Kern, C. Carbone, and H. Brune, Science **300**, 1130 (2003).
[2] F. Meier, L. Zhou, J. Wiebe, and R. Wiesendanger, Science **320**, 82 (2008).
[3] A. Lehnert, S. Dennler, P. Błoński, S. Rusponi, M. Etzkorn, G. Moulas, P. Bencok, P. Gambardella, H. Brune, and J. Hafner, Phys. Rev. B **82**, 094409 (2010).
[4] H. Brune and P. Gambardella, Surf. Sci. **603**, 1812 (2009).
[5] F. Donati, L. Gragnaniello, A. Cavallin, F. D. Natterer, Q. Dubout, M. Pivetta, F. Patthey, J. Dreiser, C. Piamonteze, S. Rusponi, and H. Brune, Phys. Rev. Lett. **113**, 177201 (2014).
[6] C. Nistor, A. Mugarza, S. Stepanow, P. Gambardella, K. Kummer, J. L. Diez-Ferrer, D. Coffey, C. de la Fuente, M. Ciria, and J. I. Arnaudas, Phys. Rev. B **90**, 064423 (2014).
[7] F. Donati, A. Singha, S. Stepanow, C. Wäckerlin, J. Dreiser, P. Gambardella, S. Rusponi, and H. Brune, Phys. Rev. Lett. **113**, 237201 (2014).
[8] A. Singha, F. Donati, C. Wäckerlin, R. Baltic, J. Dreiser, M. Pivetta, S. Rusponi, and H. Brune, Nano Lett. **16**, 3475 (2016).
[9] A. Singha, R. Baltic, F. Donati, C. Wäckerlin, J. Dreiser, L. Persichetti, S. Stepanow, P. Gambardella, S. Rusponi, and H. Brune, Phys. Rev. B **96**, 224418 (2017).
[10] F. Donati, S. Rusponi, S. Stepanow, C. Wäckerlin, A. Singha, L. Persichetti, R. Baltic, K. Diller, F. Patthey, E. Fernandes, J. Dreiser, Ž. Šljivančanin, K. Kummer, C. Nistor, P. Gambardella, and H. Brune, Science **352**, 318 (2016).
[11] R. Baltic, M. Pivetta, F. Donati, C. Wäckerlin, A. Singha, J. Dreiser, S. Rusponi, and H. Brune, Nano Lett. **16**, 7610 (2016).
[12] F. D. Natterer, K. Yang, W. Paul, P. Willke, T. Choi, T. Greber, A. J. Heinrich, and C. P. Lutz, Nature **543**, 226 (2017).
[13] F. D. Natterer, F. Donati, F. Patthey, and H. Brune, Phys. Rev. Lett. **121**, 027201 (2018).
[14] F. Donati, S. Rusponi, S. Stepanow, L. Persichetti, A. Singha, D.M. Juraschek, C. Wäckerlin, R. Baltic, M. Pivetta, K. Diller, C. Nistor, J. Dreiser, K. Kummer, E. Velez-Fort, N.A. Spaldin, H. Brune, and P. Gambardella Phys. Rev. Lett. **124**, 077204 (2020).
[15] P. R. Forrester, F. Patthey, E. Fernandes, D. P. Sblendorio, H. Brune, and F. D. Natterer, Phys. Rev. B **100**, 180405(R) (2019).
[16] W. T. Wang, J. Magn. **25**, 121 (2020).
[17] G. Y. Kim, H. R. Cha, Y. K. Baek, Y. K. Kim, D. H. Kim, Y. D. Kim, and J. G. Lee, J. Magn. **25**, 197 (2020).
[18] J. Y. Choi, H. W. Kwon, B. A. Kim, and J. G. Lee, J. Magn. **25**, 205 (2020).
[19] J. G. Yoo, H. R. Cha, D. H. Kim, Y. D. Kim, and J. G. Lee, J. Magn. **25**, 29 (2020).
[20] Z. B. Li, J. Z. Li, Z. Y. Xu, Y. F. Li, and X.-F. Zhang, J. Magn. **25**, 43 (2020).
[21] J. D. Rinehart and J. R. Long, Chem. Sci. **2**, 2078 (2011).
[22] J. Dreiser, J. Phys.: Condens. Matter **27**, 183203 (2015).
[23] Gorller-Warland and Eyring, Handbook on the physics and chemistry of rare earth, Vol. 23, Chap. 155, Elsevier, 1996.
[24] F. Donati, Q. Dubout, G. Autès, F. Patthey, F. Calleja, P. Gambardella, O. V. Yazyev, and H. Brune, Phys. Rev. Lett. **111**, 236801 (2013).
[25] I. G. Rau, S. Baumann, S. Rusponi, F. Donati, S. Stepanow, L. Gragnaniello, J. Dreiser, C. Piamonteze, F. Nolting, S. Gangopadhyay, O. R. Albertini, R. M. Macfarlane, C. P. Lutz, B. A. Jones, P. Gambardella, A. J. Heinrich, and H. Brune, Science **344**, 988 (2014).
[26] S. Baumann, F. Donati, S. Stepanow, S. Rusponi, W. Paul, S. Gangopadhyay, I. G. Rau, G. E. Pacchioni, L. Gragnaniello, M. Pivetta, J. Dreiser, C. Piamonteze, C. P. Lutz, R. M. Macfarlane, B. A. Jones, P. Gambardella, A. J. Heinrich, and H. Brune, Phys. Rev. Lett. **115**, 237202 (2015).
[27] A. Singha, F. Donati, F.D. Natterer, C. Wäckerlin, S. Stavrić, Z.S. Popović, Ž. Šljivančanin, F. Patthey, and H. Brune, Phys. Rev. Lett. **121**, 257202 (2018).
[28] R. Giraud, W. Wernsdorfer, A. M. Tkachuk, D. Mailly, and B. Barbara, Phys. Rev. Lett. **87**, 057203 (2001).
[29] N. Ishikawa, M. Sugita, and W. Wernsdorfer, J. Am. Chem. Soc. **127**, 3650 (2005).
[30] T. Miyamachi, T. Schuh, T. Märkl, C. Bresch, T. Balashov, A. Stöhr, C. Karlewski, S. André, M. Marthaler, M. Hoffmann, M. Geilhufe, S. Ostanin, W. Hergert, I. Mertig, G. Schön, A. Ernst, and W. Wulfhekel, Nature **503**, 242 (2013).
[31] C. Hübner, B. Baxevanis, A. A. Khajetoorians, and D. Pfannkuche, Phys. Rev. B **90**, 155134 (2014).
[32] M. Marciani, C. Hübner, and B. Baxevanis, Phys. Rev. B **95**, 125433 (2017).
[33] R. Sessoli, D. Gatteschi, A. Caneschi, and M. A. Novak, Nature (London) **365**, 141 (1993).
[34] D. Gatteschi and R. Sessoli, Angew. Chem. Int. Ed. Engl. **42**, 268 (2003).
[35] M. Mannini, F. Pineider, C. Danieli, L. Totti, F. Sorace, P. Sainctavit, M.-A. Arrio, E. Otero, L. Joly, J. C. Cezar, A. Cornia, and R. Sessoli, Nature (London) **468**, 417 (2010).
[36] A. Abragam and B. Bleaney, Electron Paramagnetic Resonance of Transition Ions, Clarendon Press, Oxford, (1970).

[37] C. A. P. Goodwin, F. Ortu, D. Reta, N. F. Chilton, and D. P. Mills, Nature (London) **548**, 439 (2017).
[38] F.-S. Guo, B. M. Day, Y.-C. Chen, M.-L. Tong, A. Mansikkamaki, and R. A. Layfield, Science **362**, 1400 (2018).
[39] A. Lunghi, F. Totti, R. Sessoli, and S. Sanvito, Nat. Commun. **8**, 14620 (2017).
[40] L. Escalera-Moreno, J. J. Baldoví, A. Gaita-Ariño, and E. Coronado, Chem. Sci. **9**, 3265 (2018).
[41] S. Roychoudhury and S. Sanvito, Phys. Rev. B **98**, 125204 (2018).
[42] G. Binnig, H. Rohrer, Ch. Gerber, and E. Weibel, Phys. Rev. Lett. **49**, 57 (1982).
[43] J. Pal, M. Smerieri, E. Celasco, L. Savio, L. Vattuone, and M. Rocca, Phys. Rev. Lett. **112**, 126102 (2014).
[44] E. Fernandes, F. Donati, F. Patthey, S. Stavric, Z. Sljivancanin, and H. Brune, Phys. Rev. B **96**, 045419 (2017).
[45] C. Piamonteze, U. Flechsig, S. Rusponi, J. Dreiser, J. Heidler, M. Schmidt, R. Wetter, M. Calvi, T. Schmidt, H. Pruchova, J. Krempasky, C. Quitmann, H. Brune, and F. Nolting, J. Synchrotron Radiat. **19**, 661 (2012).
[46] K. Kummer, A. Fondacaro, E. Jimenez, E. Velez-Fort, A. Amorese, M. Aspbury, F. Yakhou-Harris, P. van der Linden, and N. B. Brookes, J. Synchrotron Radiat. **23**, 464 (2016).
[47] N. Ishikawa, M. Sugita, T. Ishikawa, S.-y. Koshihara, and Y. Kaizu, J. Am. Chem. Soc. **125**, 8694 (2003).
[48] R. Westerström, J. Dreiser, C. Piamonteze, M. Muntwiler, S. Weyeneth, H. Brune, S. Rusponi, F. Nolting, A. Popov, S. Yang, L. Dunsch, and T. Greber, J. Am. Chem. Soc. **134**, 9840 (2012).
[49] J. M. Zadrozny, D. J. Xia, M. Atanasov, G. J. Long, F. Grandjean, F. Neese, and J. R. Long, Nat. Chem. **5**, 577 (2013).
[50] L. Ungur, J. J. Le Roy, I. Korobkov, M. Murugesu, and L. F. Chibotaru, Angew. Chem. Int. Ed. **53**, 4413 (2014).
[51] F. Pointillart, K. Bernot, S. Golhen, B. Le Guennic, T. Guizouarn, L. Ouahab, and O. Cador, Angew. Chem. Int. Ed. **54**, 1504 (2015).
[52] Y.-C. Chen, J.-L. Liu, L. Ungur, J. Liu, Q.-W. Li, L.-F. Wang, Z.-P. Ni, L. F. Chibotaru, X.-M. Chen, and M.-L. Tong, J. Am. Chem. Soc. **138**, 2829 (2016).
[53] R. Wiesendanger, Rev. Mod. Phys. **81**, 1495 (2009).
[54] S. Loth, C. P. Lutz and A. J. Heinrich, New J. Phys. **12**, 125021 (2010).
[55] L. Ungur and L. F. Chibotaru, Inorg. Chem. **55**, 10043 (2016).
[56] J. Dreiser, R. Westerström, C. Piamonteze, F. Nolting, S. Rusponi, H. Brune, S. Yang, A. Popov, L. Dunsch, and T. Greber, Appl. Phys. Lett. **105**, 032411 (2014).
[57] C. Wäckerlin, F. Donati, A. Singha, R. Baltic, S. Rusponi, K. Diller, F. Patthey, M. Pivetta, Y. Lan, S. Klyatskaya, M. Ruben, H. Brune, and J. Dreiser, Adv. Mater. **28**, 5195 (2016).
[58] D. L. Mills, Phys. Rev. **146**, 336 (1966).
[59] R. Vincent, S. Klyatskaya, M. Ruben, W. Wernsdorfer, and F. Balestro, Nature **488**, 357 (2012).
[60] S. Thiele, F. Balestro, R. Ballou, S. Klyatskaya, M. Ruben, and W. Wernsdorfer, Science **344**, 1135 (2014).
[61] M. Studniarek, C. Wäckerlin, A. Singha, R. Baltic, K. Diller, F. Donati, S. Rusponi, H. Brune, Y. Lan, S. Klyatskaya, M. Ruben, A. P. Seitsonen, and J. Dreiser, Adv. Sci. **6**, 1901736 (2019).
[62] R. Baltic, F. Donati, A. Singha, C. Wäckerlin, J. Dreiser, B. Delley, M. Pivetta, S. Rusponi, and H. Brune, Phys. Rev. B **98**, 024412 (2018).
[63] M. Pivetta, S. Rusponi, and H. Brune, Phys. Rev. B **98**, 115417 (2018).
[64] M. Pivetta, F. Patthey, I. Di Marco, A. Subramonian, O. Eriksson, S. Rusponi, and H. Brune, Phys. Rev. X **10**, 031054 (2020).